Supplementary Information for

Locking of poly (sodium acrylate) hydrogels for underwater ultra-stretchability but overwater non-flexibility

Baibin Yang, Peipei Ma, Ting You, Bingquan Ding, Caihong Wang, Qiang Zhao, Yong Wu, Shuai Tan*

School of Chemical Engineering, Sichuan University, No. 24 South 9 Section 1, Yihuan Road, Chengdu 610065, China

METHODS

Chemicals

All chemical reagents and solvents were purchased from Chron Chemicals and Macklin Biochemical Technology company, which were used without further purification. Deionized water was applied for hydrogel preparation.

Characterization

The scanning electron microscope (SEM) observations and energy dispersive spectra of the freeze-dried samples were performed by a Tescan Mira LMS field emission SEM at an accelerating voltage of 5 keV. The Fourier transform infrared (FT-IR) spectra were measured with the use of a Nicolet IS50 FT-IR spectrometer. The Raman spectra were measured by a DXR3 laser confocal Raman spectrometer with the excitation wavelength of 785 nm. The X-ray photoelectron spectroscopy (XPS) was performed using a Thermo Fisher K-ALPHA spectrometer with a monochromatic Al Kα X-ray source (h_v = 1486.8 eV). The binding energy scale was calibrated using the adventitious carbon peak (C 1s = 284.8 eV) as a reference.

Before measurements, the hydrogel was freeze-dried under vacuum to a constant weight in a Christ Alpha 1-2LD vacuum freeze dryer. XRD analyses were carried out by a Rigaku Ultima IV diffractometer, using Cu-Kα radiation at 40 kV and 40 mA. Static contact angle observations were obtained using the OSA60 Contact Angle Gauge.

The water content of the hydrogels was tested by placing them in a vacuum oven at 60°C until their mass no longer changed. The swelling behavior of the hydrogels was tested by immersing the hydrogel networks in specific solutions and weighing them at a fixed time. The drying behavior of the hydrogels was tested by immersing the hydrogel networks in air and weighing them at a fixed time.

The mechanical performance of the hydrogels was measured using an Instron 68TM-50 electronic universal test machine. All the tests for the mechanical performance of the hydrogels were performed at room conditions (15~25 ℃, 70~85% relative humidity) without special measures to avoid dehydration of the hydrogels. The compression tests of the samples were performed with a displacement rate of 3 mm min^{-1}. Cylindrical specimens with a size of ø6×6 mm were prepared to perform uniaxial compression tests. In the cyclic compression tests, the crosshead returned to its original position immediately with a displacement rate of 3 mm min^{-1} after the sample was compressed to an 80% compressive strain with no recovery time. The tension tests of the samples were performed with a displacement rate of 100 mm min^{-1}. In the cyclic tension tests, the crosshead returned to its original position immediately with a displacement rate of 100 mm min^{-1} after the sample was stretched to a 1500% tensile strain with no recovery time. The toughness during the tension process of the hydrogels was calculated by integrating the area under the stress-strain curve.

The resistance change of the hydrogels under different deformations or different environments was recorded by a KEITHLEY DMM6500 6 1/2 digit multimeter.

Molecular dynamics simulation

The MD simulation of PANa-0.6Ca hydrogel, PANa-2Ca hydrogel, PANa-0.6Ca hydrogel (in more water), and PANa-2Ca hydrogel (in more water) were performed on Materials Studio, accomplished by using the Compass II force field in the Forcite Plus modules. The simulation methods of all the samples were the same. The four systems were modeled separately. Poly (sodium acrylate) chains consisting of 10 repeated monomers were applied as the polymer chains in the hydrogels, and the covalent crosslinking in all the hydrogels was not considered during the MD simulations. For the PANa-0.6Ca hydrogel, the polymer chains, $CaCl_2$, and H_2O were added in a three-dimensional periodic lattice of 18.8 Å × 18.8 Å × 18.8 Å with a number of 2, 4, and 160, respectively, which was consistent with the actual molecular ratio of PANa-0.6Ca hydrogels. For the PANa-2Ca hydrogel, the polymer chains, $CaCl_2$, and H_2O were added in a three-dimensional periodic lattice of 18.8 Å × 18.8 Å × 18.8 Å with a number of 2, 4, and 160, respectively, which was also consistent with the actual ratio of hydrogels. For the PANa-0.6Ca hydrogel (in more water), the PANa chain, $CaCl_2$ and H_2O were added in a three-dimensional periodic lattice of 27.6 Å × 27.6 Å × 27.6 Å with the number of 2, 4 and 640, respectively. For the PANa-2Ca hydrogel (in more water), the PANa chain, $CaCl_2$ and H_2O were added in a three-dimensional periodic lattice of 27.6 Å × 27.6 Å × 27.6 Å with the number of 2, 14 and 640, respectively. The energy of the simulated box was optimized by geometry optimization with the number of convergence steps set to 5000. The simulation was performed in canonical ensemble (NVT) with a constant temperature and volume, where the temperature was controlled to be 298 K by the Nose-Hoover Langevin (NHL) thermostat. Then, the simulation was

accomplished with a relaxation time of 5 ns. The coordination number (CN) between different atoms was calculated by the following expression[46]:

$$CN = \int_0^r 4\pi r^2 \rho g(r) dr \quad (1)$$

where ρ, $g(r)$, and r represent the number density of coordination atoms, the radial distribution function, and the distance between the coordination atom and the reference atom.

Hydrogel preparation (PANa-xCa and PANa-yCa)

The as-prepared PANa hydrogels were one-step prepared via in-situ polymerization of sodium acrylate monomer (AANa, 4.5 mol L^{-1}) and DVB (crosslinker, 0.2 mol L^{-1}) aqueous solutions. The aqueous solutions were ultrasonically oscillated for 1 h before polymerization for the homogenous dispersion of DVB. The solution was cooled to room temperature and injected into specific shaped polytetrafluoroethylene molds and the polymerization was initiated by ammonium persulfate (KPS, 0.0004 mol L^{-1}) at 60°C. After 4h, transparent as-prepared PANa hydrogels were obtained. The PANa-xCa and PANa-yCa hydrogels were then prepared by simply immersing the PANa precursor at a specific weight into $CaCl_2$ solutions (50 times in weight to PANa precursor) at different concentrations (x = 0.2, 0.4, 0.6, 0.8 mol L^{-1} and y = 1, 2, 4 mol L^{-1}) for 24 h to reach the equilibrium state.

The reference hydrogels (PANa-0.6M $Ca(NO_3)_2$ and PANa-0.6M $FeCl_3$) were prepared similarly to the PANa-0.6Ca hydrogels by replacing the 0.6 mol L^{-1} $CaCl_2$ solutions with 0.6 mol L^{-1} $Ca(NO_3)_2$ or $FeCl_3$ solutions.

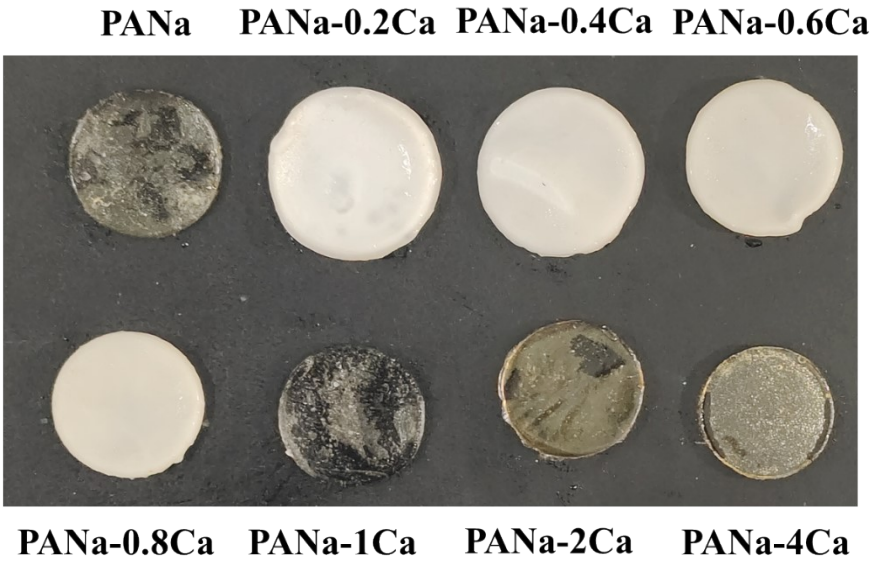

Figure S1. Images of as-prepared PANa, PANa-xCa (x=0.2, 0.4, 0.6, and 0.8 mol L^{-1}) and PANa-yCa (y=1, 2, and 4 mol L^{-1}) hydrogels.

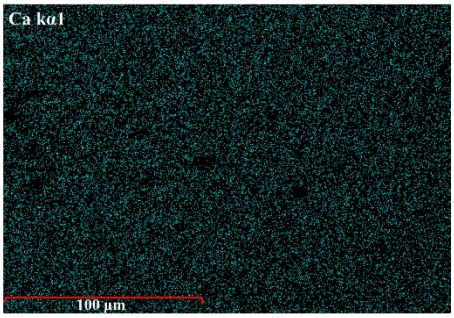

Figure S2. EDS mapping of elemental Ca in PANa-0.6Ca hydrogels.

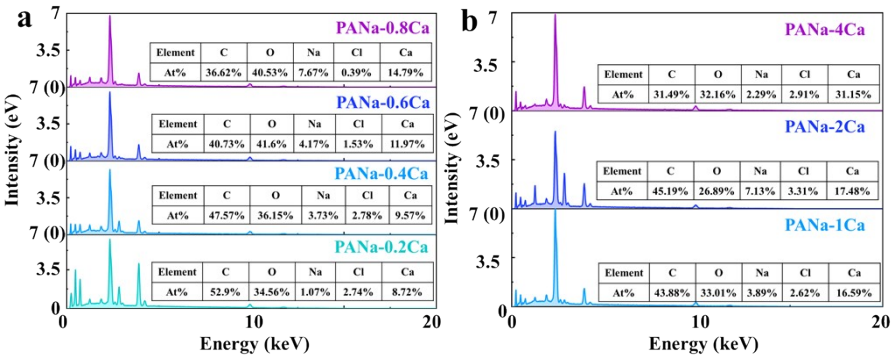

Figure S3. (a) Elemental distribution of PANa-xCa hydrogels. (b) Elemental distribution of PANa-yCa hydrogels.

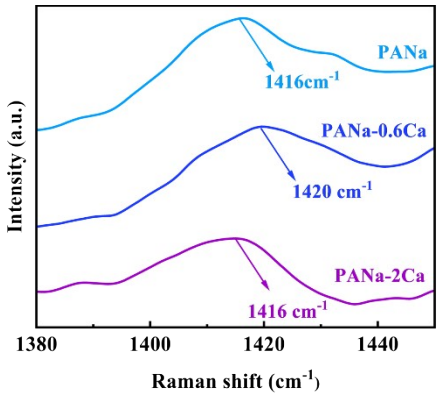

Figure S4. Raman spectra of PANa, PANa-0.6Ca, and PANa-2Ca hydrogels.

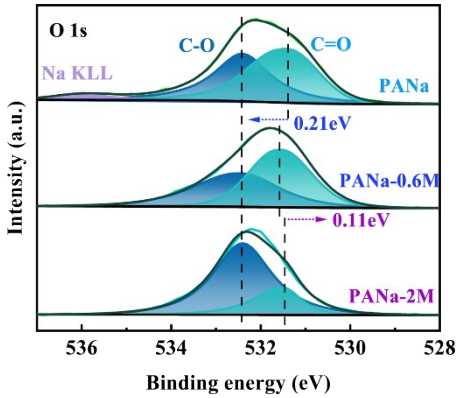

Figure S5. The high-resolution O 1s XPS spectra of PANa, PANa-0.6Ca, and PANa-2Ca hydrogels.

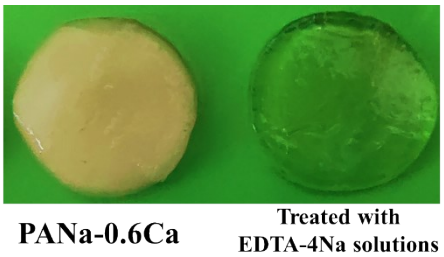

Figure S6. Images of PANa-0.6Ca hydrogels and PANa-0.6Ca hydrogels treated with EDTA-4Na solutions.

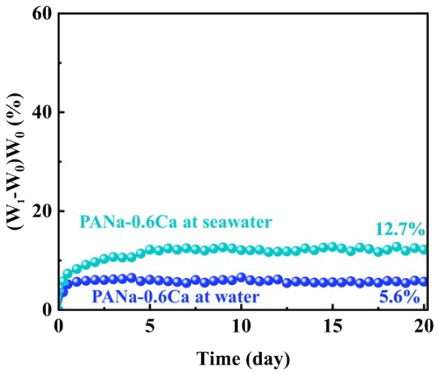

Figure S7. The swelling behavior of PANa-0.6Ca in water and seawater for 20 days.

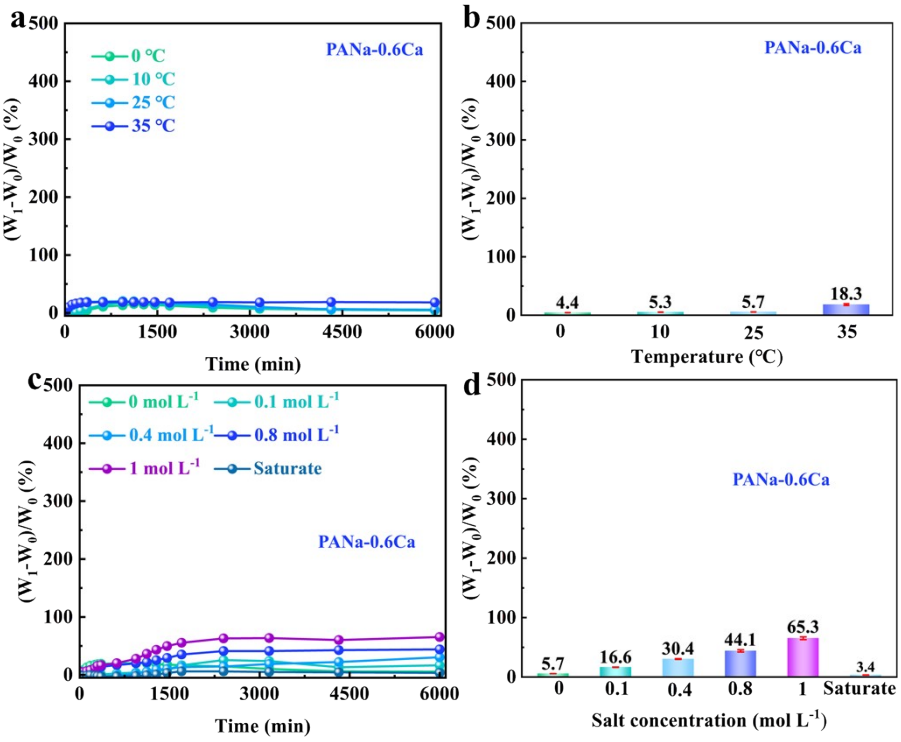

Figure S8. (a) The swelling behavior of PANa-0.6Ca hydrogels at different water temperatures. (b) The equilibrium swelling rates of PANa-0.6Ca hydrogels at different water temperatures. (c) The swelling behavior of PANa-0.6Ca hydrogels at different salt concentrations. (d) The equilibrium swelling rates of PANa-0.6Ca hydrogels at different salt concentrations.

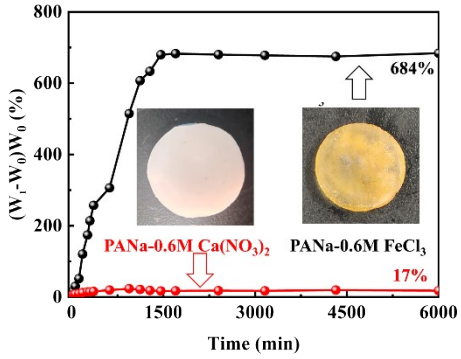

Figure S9. The swelling behavior of PANa-0.6M $Ca(NO_3)_2$ (PANa treated by 0.6 mol L^{-1} $Ca(NO_3)_2$) and PANa-0.6M $FeCl_3$ (PANa treated by 0.6 mol L^{-1} $FeCl_3$) hydrogels in water. W_0: initial weight, W_1: weight at a specific time.

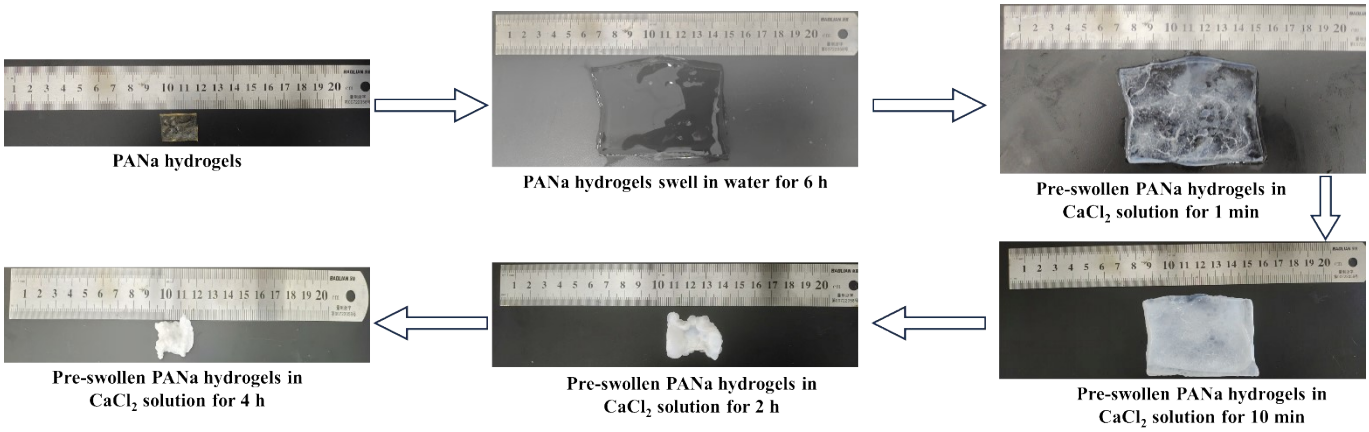

Figure S10. Physical images of PANa hydrogels swelling in water, then being immersed in 0.6 mol L^{-1} $CaCl_2$ solutions.

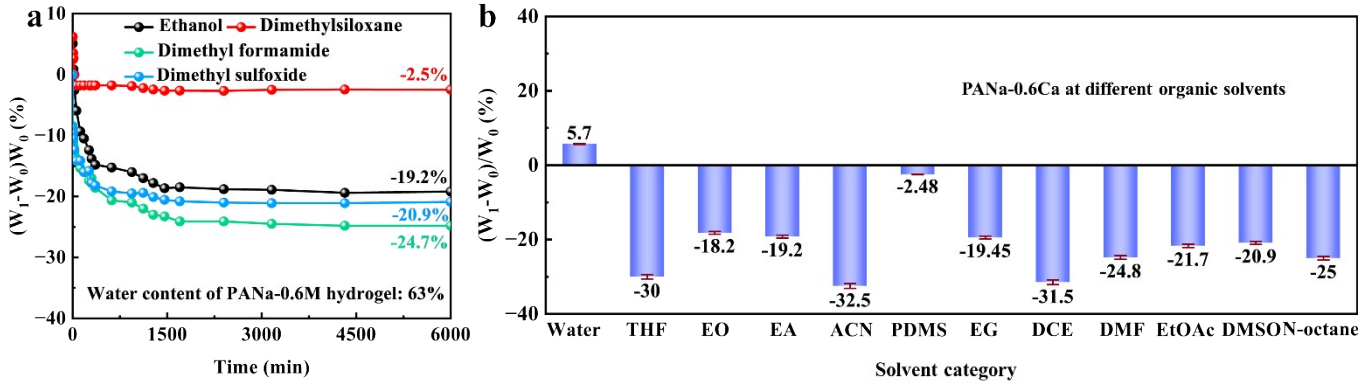

Figure S11. Organic solvent tolerance of PANa-0.6M hydrogels. (a) The swelling behavior of PANa-0.6Ca hydrogels in ethanol, dimethyl siloxane, *N,N*-Dimethyl formamide, dimethyl sulfoxide. (b) The swelling equilibrium ratio of PANa-0.6Ca hydrogels in different organic solvents. (W_0: initial weight, W_1: weight at specific time).

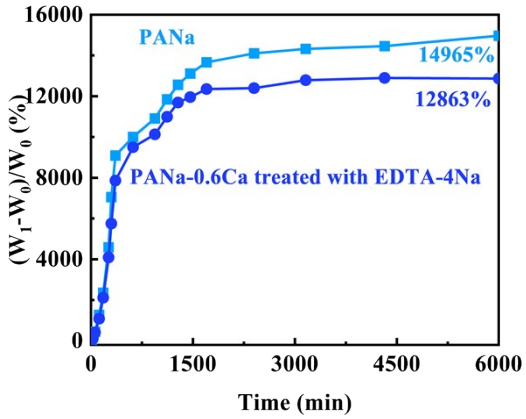

Figure S12. The swelling behavior of PANa-0.6Ca hydrogels after being treated with EDTA-4Na solutions. W_0: initial weight, W_1: weight at a specific time.

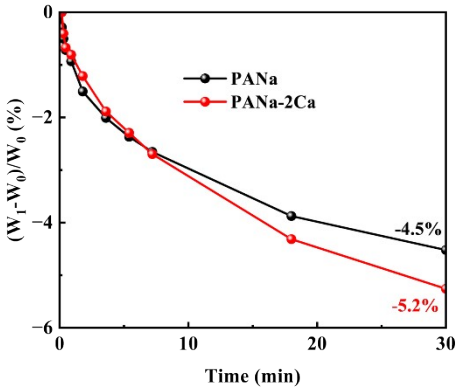

Figure S13. Weight change of PANa and PANa-2Ca hydrogels in air for 30 mins. W_0: initial weight, W_1: weight at a specific time.

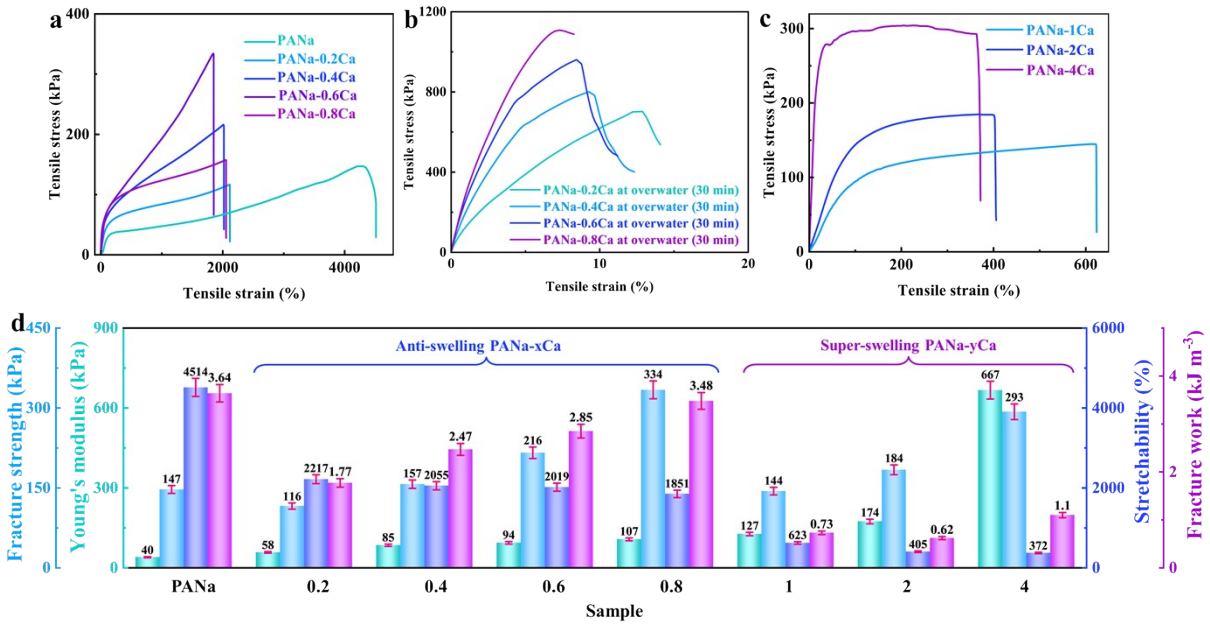

Figure S14. (a) The tensile stress-strain curves of as-prepared PANa and PANa-xCa hydrogels. (b) The tensile stress-strain curves of PANa-0.6Ca at overwater conditions for 30 mins. (c) The tensile behavior of PANa-yCa hydrogels. (d) The Young's modulus, stretchability, fracture strength, and fracture work of PANa, PANa-xCa, and PANa-yCa hydrogels.

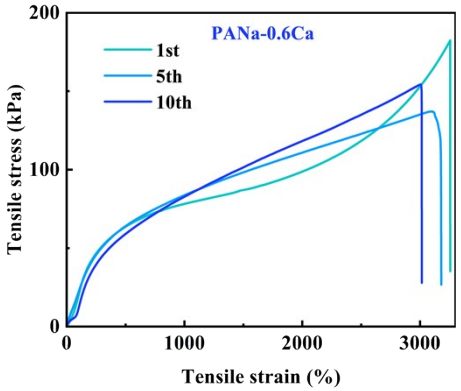

Figure S15. The tensile strain-stress curves of PANa-0.6Ca hydrogels under the cycles of hydration and dehydration.

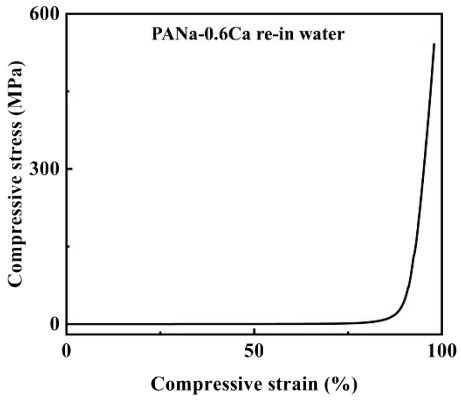

Figure S16. The compressive stress-strain curves of PANa-0.6Ca re-entering water.

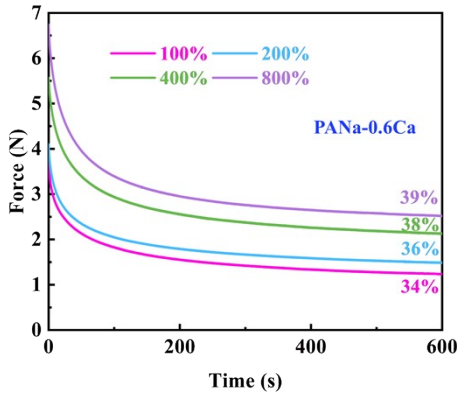

Figure S17. Stress relaxation testing of PANa-0.6Ca$_{eq}$ hydrogels.

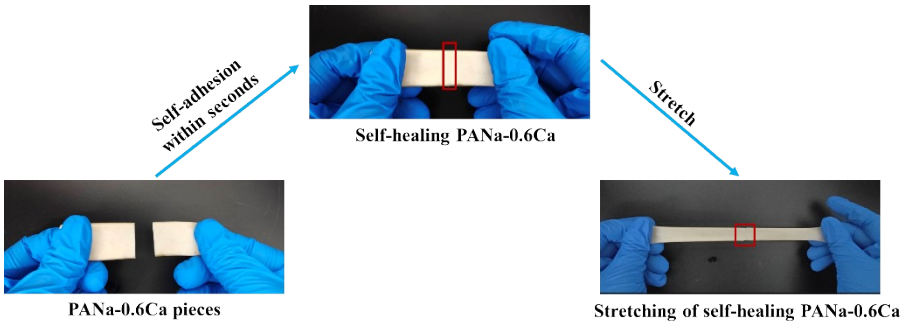

Figure S18. Physical images of self-healing for PANa-0.6Ca hydrogels within seconds.

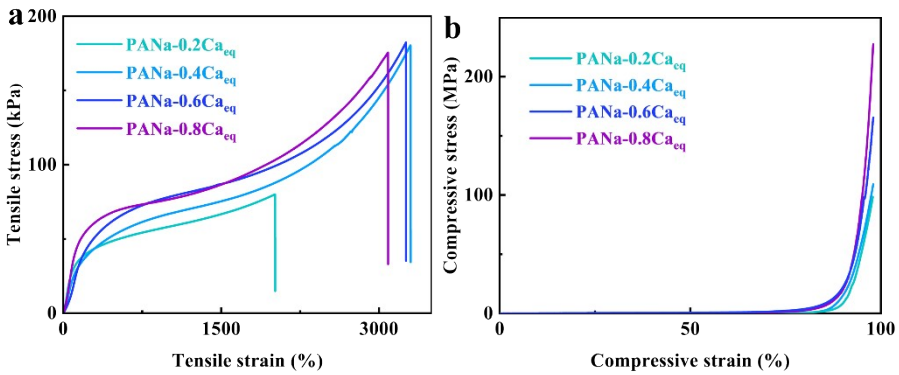

Figure S19. Mechanical properties of PANa-xCa_{eq} hydrogel. (a) The tensile stress-strain curves of PANa-xCa_{eq} hydrogels. (b) The compressive stress-strain curves of PANa-xCa_{eq} hydrogels.

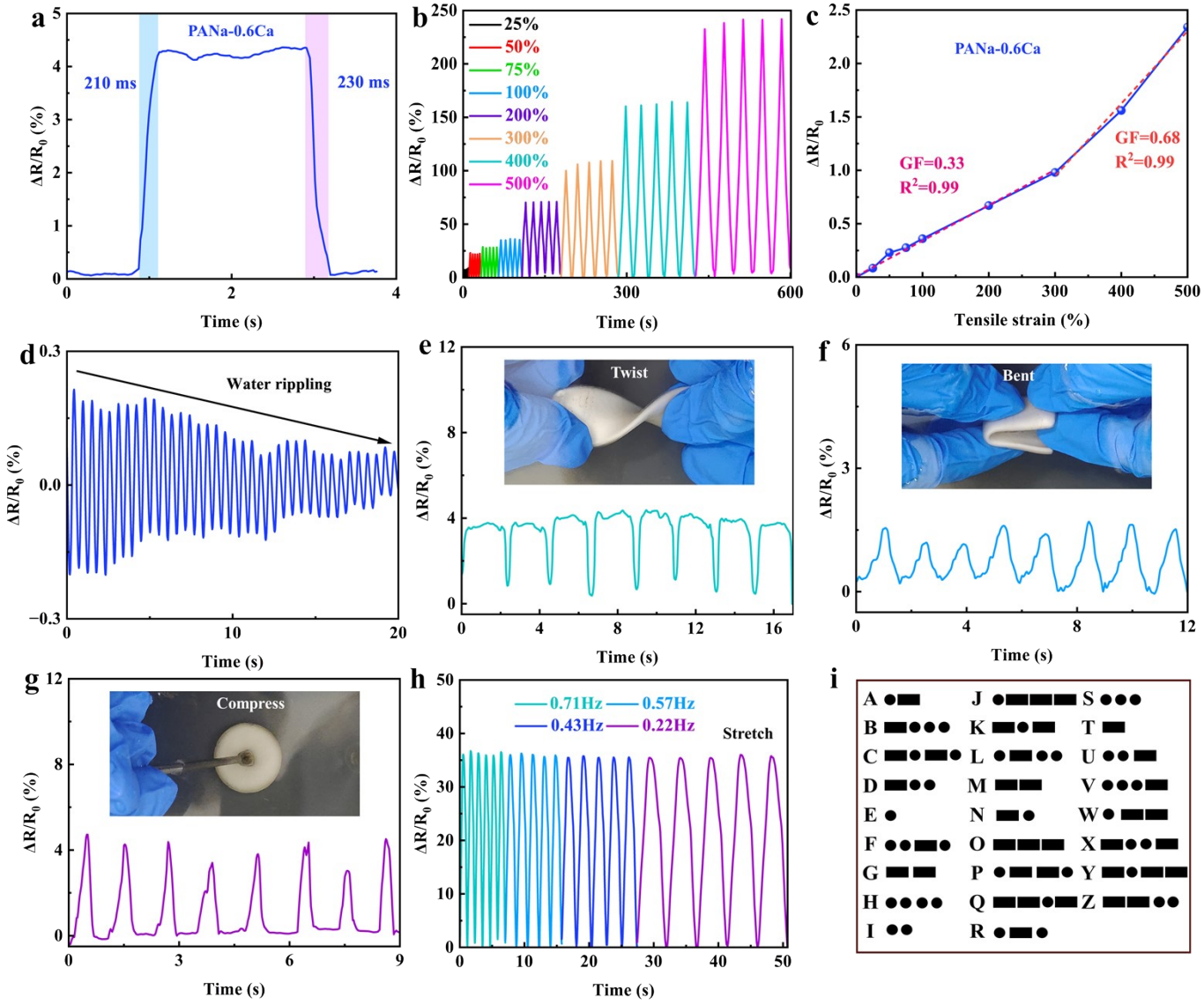

Figure S20. Sensing performance of PANa-0.6Ca hydrogels. (a) Response and recovery time of sensor based on the PANa-0.6Caeq hydrogels. (b) Relative resistance change of the PANa-0.6Caeq hydrogels during cyclic tensile deformation at different strains. (c) Relative resistance change as a function of tensile strains. (d) PANa-0.6Ca_{eq} hydrogel sensors monitored water wave changes. (e-h) Relative resistance changes of PANa-0.6Ca_{eq} hydrogels during deformation: (e) twist, (f) bent, (g) compress. (h) Relative resistance changes of PANa-0.6Ca_{eq} hydrogels at different frequencies. (i) The diagram illustrating of Morse code transmits information.

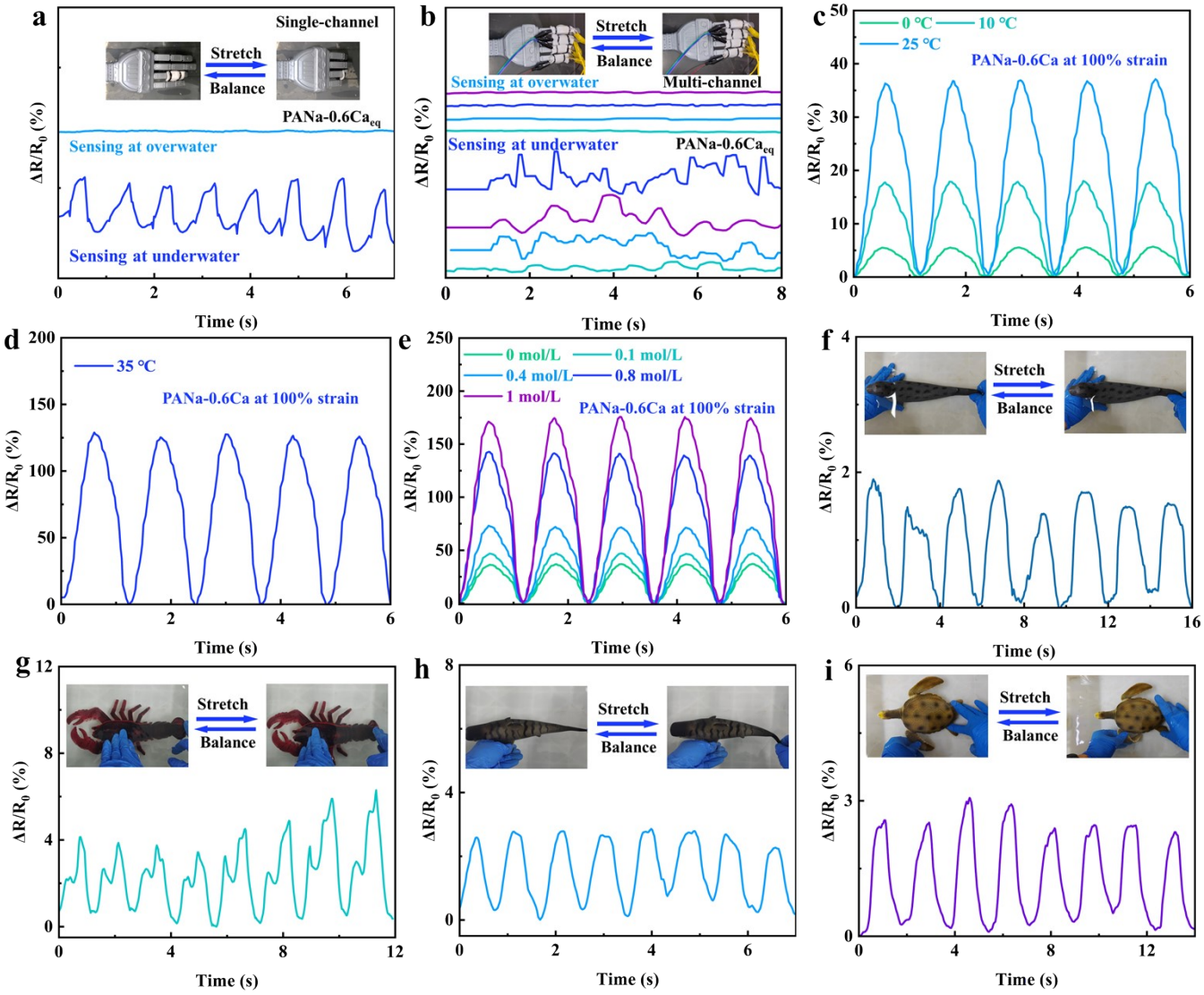

Figure S21. Sensing applications of PANa-0.6Ca hydrogels specific for underwater conditions. (a) Relative resistance changes of PANa-0.6Ca$_{eq}$ hydrogels during single-channel robotic hand motion at overwater and underwater conditions. (b) Relative resistance changes of PANa-0.6Ca$_{eq}$ hydrogels during multi-channel robotic hand motion at overwater and underwater conditions. (c) Relative resistance changes of PANa-0.6Ca$_{eq}$ hydrogels at different temperatures under 100% strain. (d) Relative resistance changes of PANa-0.6Ca$_{eq}$ hydrogels at 35°C under 100% strain. (e) Relative resistance changes of PANa-0.6Ca$_{eq}$ hydrogels at different salt concentrations under 100% strain. (f-i) Relative resistance changes of PANa-0.6Ca$_{eq}$ hydrogels for motion monitoring of marine animal models: (f) seal, (g) lobster, (h) fish, and (i) turtle.

Table S1. The Young's modulus, stretchability, fracture strength, and fracture work of PANa-xCa, PANa-yCa hydrogels at underwater and PANa-xCa hydrogels at overwater conditions for 30 mins.

Sample	Underwater [a]				Overwater [b]			
	Fracture strength (kPa)	Young's modulus (kPa)	Stretchability (%)	Fracture work (kJ m^{-3})	Fracture strength (kPa)	Young's modulus (kPa)	Stretchability (%)	Fracture work (kJ m^{-3})
PANa	147	40	4514	3641	160	43	4091	4133
PANa-0.2Ca	116	58	2217	1772	702	709	12.9	638
PANa-0.4Ca	157	85	2055	2468	800	1286	9.2	672
PANa-0.6Ca	216	94	2019	2849	961	1728	8.4	733
PANa-0.8Ca	334	107	1851	3489	1108	1857	7.3	623
PANa-1Ca	144	127	623	734	-	-	-	-
PANa-2Ca	184	174	405	620	-	-	-	-
PANa-4Ca	293	667	372	111	-	-	-	-

[a] hydrogels at underwater, [b] hydrogels at overwater conditions for 30 mins, [c] -: No data.

Table S2. Comparison of stretchability and water content between PANa-0.6Ca_{eq} hydrogels and reported anti-swelling hydrogels based on versatile strategies.

Refs	Hydrogels	Stretchability (%)	Water content (%)
S1	Ionic coordination hydrogels	441	88
S2		900	70
S3		200	60
S4	Hydrophobic association hydrogels	520	72
S5		1200	62
S6		120	87
S7	Double-network hydrogels	520	82
S8		451	85
S9		33	50
S10	Nanocomposite hydrogels	1200	59
S11		100	63
S12		6	50
S13	Multiple crosslinking hydrogels	350	38
S14		1460	70
S15		300	90
S16	Other strategies for hydrogels	300	92
S17		900	65
S18		50	60
This work		**3000**	**70**

Reference

(S1) Jiao, Z.; Gao, W.; Wang, L.; Wei, Y.; Guo, H.; Yuan, X.; Zhao, J. Mechanically adaptable and highly anti-swelling hydrogel enabled by competitive and synergistic ion training for motion monitoring and underwater encryption. *Chem. Eng. J.* **2025**, *519*, 164953.

(S2) Pi, M.; Qin, S.; Wen, S.; Wang, Z.; Wang, X.; Li, M.; Lu, H.; Meng, Q.; Cui, W.; Ran, R. Rapid Gelation of Tough and Anti-Swelling Hydrogels under Mild Conditions for Underwater Communication. *Adv. Funct. Mater.* **2022**, *33*(1), 2416425.

(S3) Huang, Y.; Qian, S.; Zhou, J.; Chen, W.; Liu, T.; Yang, S.; Long, S.; Li, X. Achieving Swollen yet Strengthened Hydrogels by Reorganizing Multiphase Network Structure. *Adv. Funct. Mater.* **2023**, *33*(22), 2213549.

(S4) Ren, J.; Chen, G.; Yang, H.; Zheng, J.; Li, S.; Zhu, C.; Yang, H.; Fu, J. Super-Tough, Non-Swelling Zwitterionic Hydrogel Sensor Based on the Hofmeister Effect for Potential Motion Monitoring of Marine Animals. Adv. Mater. **2024**, *36*(48), 2412162.

(S5) Shen, K.; Lv, Z.; Yang, Y.; Wang, H.; Liu, J.; Chen, Q.; Liu, Z.; Zhang, M.; Liu, J.; Cheng, Y. A Wet-Adhesion and Swelling-Resistant Hydrogel for Fast Hemostasis, Accelerated Tissue Injury Healing and Bioelectronics. *Adv. Mater.* **2024**, *37*(6), 2414092.

(S6) Bian, S.; Hao, L.; Qiu, X.; Wu, J.; Chang, H.; Kuang, G. M.; Zhang, S.; Hu, X.; Dai, Y.; Zhou, Z.; Huang, F.; Liu, C.; Zou, X.; Liu, W.; Lu, W. W.; Pan, H.; Zhao, X. An Injectable Rapid-Adhesion and Anti-Swelling Adhesive Hydrogel for Hemostasis and Wound Sealing. *Adv. Funct. Mater.* **2022**, *32*(46), 2207741.

(S7) Li, X.; Wang, J.; Guo, Y.; Qian, H.; Chen, Y.; Chen, Y.; Wang, J.; Wang, Y.; Martins, M. C. L.; Hu, X.; Wang, J. a.; Ji, J. Non-swelling polyelectrolyte complex hydrogels with tissue-matchable mechanical properties for versatile wet wound closure. *Composites, Part B* **2024**, *279*, 111456.

(S8) Liu, X.; Sun, Y.; Wang, J.; Kang, Y.; Wang, Z.; Cao, W.; Ye, J.; Gao, C. A tough, antibacterial and antioxidant hydrogel dressing accelerates wound healing and suppresses hypertrophic scar formation in infected wounds. *Bioact. Mater.* **2024**, *34*, 269-281.

(S9) Lan, Z.; Wang, Y.; Hu, K.; Shi, S.; Meng, Q.; Sun, Q.; Shen, X. Anti-swellable cellulose hydrogel for underwater sensing. *Carbohydr. Polym.* **2023**, *306*, 120541.

(S10) Wang, H.; Lin, X.; Li, X.; Lv, D.; Zhang, J.; Wei, L.; Tang, J.; Lin, Y.; Wu, X.; Xu, X. Antiswelling, Ultrastretchable, and Ultrastable Hydrogel Sensors for Long-Term Underwater Monitoring. *Small* **2025**, *21*(27), 2503067.

(S11) Li, F.; Zhang, G.; Wang, Z.; Jiang, H.; Feng, X.; Yan, S.; Zhang, L.; Li, H.; Zhao, T.; Liu, M. Bioinspired nonswellable ultrastrong nanocomposite hydrogels with long-term underwater superoleophobic behavior. *Chem. Eng. J.* **2019**, *375*, 122047.

(S12) Lin, C.; Jia, W.; Chang, L.; Ren, G.; Hu, S.; Sui, X.; Gao, L.; Sui, K.; Jiang, L. Anti-Swelling 3D Nanohydrogel for Efficient Osmotic Energy Conversion. *Adv. Funct. Mater.* **2024**, *35*(10), 2416425.

(S13) Liu, Z.; Liu, Z.; Shu, B.; Lian, C.; Wu, J.; Wen, Q.; Wu, J.; Yang, Z.; Zhou, W.; Hu, Y. One-pot preparation of tough, anti-swelling, antibacterial and conductive multiple-crosslinked hydrogels assisted by phytic acid and ferric trichloride. *J. Appl. Polym. Sci.* **2023**, *140*(32), 54243.

(S14) Wang, C.; Luo, Y.; Cao, X.; Li, B.; Luo, Z. Supramolecular polyurea hydrogels with anti-swelling capacity, reversible thermochromic properties, and tunable water content and mechanical performance. *Polymer* **2021**, *233*, 124213.

(S15) Qiu, J.; Kang, X.; Liu, T.; Liu, J.; Liu, H.; Zhao, X.; Li, Y.; Liu, Q.; Nong, Z.; Wang, Q.; Liu, Z. A non-swellable, anisotropic hydrogel patch with superior mechanical stability for internal anti-adhesion via physical barrier and inflammation regulation. *Mater. Today Bio* **2025**, *33*, 102017.

(S16) Xue, H.; Yi, D.; Wang, J.; Li, Z.; Jiang, Y.; Ma, S.; Peng, W.; He, Y.; Mao, H.; Gu, Z. Rapid Gelation of Anti-Swelling, Self-Healing, and Biocompatible PEG Hydrogels Based on CBT-Cys Click Reaction under Mild Conditions. *ACS Macro Lett.* **2025**, *14*(5), 664-670.

(S17) Jiang, L.; Li, F.; Li, Y.; Pi, M.; Xie, J.; Zhang, J.; Guo, H.; Ran, R.; Cui, W. Solvent-Free Fabrication of Robust Physical Hydrogels via Bulk Copolymerization for Underwater Acoustics. *Adv. Mater.* **2025**, 2508162.

(S18) Zhang, H.; Zhao, T.; Duffy, P.; Dong, Y.; Annaidh, A. N.; O'Cearbhaill, E.; Wang, W. Hydrolytically Degradable Hyperbranched PEG-Polyester Adhesive with Low Swelling and Robust Mechanical Properties. *Adv. Healthcare Mater.* **2015**, *4*(15), 2260-2268.

Supplementary Video 1.

Stretching of PANa-0.6Ca hydrogel at underwater conditions and at overwater conditions after 30 mins.

Supplementary Video 2.

PANa-0.6Ca hydrogel sensor monitoring motions of an electric shark toy in seawater.